Recrystallization and texture evolution of warm-pilgered FeCrAl alloy tube during annealing at 850°C

Journal of Nuclear Materials 562 (2022) 153575

Contents lists available at ScienceDirect

Journal of Nuclear Materials

journal homepage: www.elsevier.com/locate/jnucmat

Recrystallization and texture evolution of warm-pilgered FeCrAl alloy tube during annealing at 850°C

Xiao Qin[a,b], Zhe Liu[a], Huiqun Liu[a,*], Ruiqian Zhang[c,**], Qiangfu Pan[c], Yurong Wang[c], Jingyuan Pei[c]

[a] School of Materials Science and Engineering, Central South University, Changsha 410083, China
[b] Department of Industrial and Materials Science, Chalmers University of Technology, Gothenburg, 41296, Sweden
[c] Nuclear Power Institute of China, Chengdu, Sichuan 610213, China

ARTICLE INFO

Article history:
Received 29 November 2021
Revised 24 January 2022
Accepted 29 January 2022
Available online 2 February 2022

Keywords:
FeCrAl alloy
Microstructure
Texture
EBSD
Recrystallization

ABSTRACT

Recrystallization annealing of warm-pilgered FeCrAl tubes was the key to reduce the cracking and control the microstructure and properties of the cladding tube. The recrystallization and texture evolution of warm-pilgered FeCrAl tubes were investigated. The recrystallization kinetics and textural evolution during annealing were characterized using microhardness measurements and electron backscatter diffraction. The 3D-microstructure of the warm-pilgered FeCrAl tube exhibited heterogeneous deformed grains of α-fiber and γ-fiber orientation. The significant anisotropy results in different recrystallization kinetics in the axial and circumferential directions of the tube. The mirostructure maintains a stable grain size of ~22 μm and an aspect ratio of 1.8 in the axial and circumferential directions within 0–600 min annealing time. The stable microstructure is due to the dispersion of fine Laves phase particles in the ferrite matrix. Quantitative texture analysis shows that the α-fiber texture decreased significantly and the γ-fiber increased after recrystallization. During the annealing process, the α-fiber strong point texture component {112}<110> turns into {223}<110> and the γ-fiber component {111}<110> turns into {111}<112>. The recrystallization and texture evolution of warm-pilgered FeCrAl tube is of great significance to preparation and microstructure control of final cladding tube.

1. Introduction

Iron-chromium-aluminum (FeCrAl) alloys are widely used for heating elements due to their low cost, high thermal conductivity, and excellent high-temperature properties [1–3]. More importantly, FeCrAl alloys have excellent accident resistance owing to their unparalleled oxidation and corrosion resistance under high temperatures conditions [4,5]. Following the Fukushima Daiichi nuclear accident, researchers began considering FeCrAl alloys as an alternative to zirconium alloys as an accident tolerant fuel (ATF) cladding material for light water reactors (LWRs) [6–8].

FeCrAl alloys contain major alloying elements Fe (matrix), Cr (10–15 wt%), and Al (4–7.5 wt%) as well as other minor alloying elements (Mo, Nb, and Zr), which were added to improve the strength and optimize the microstructure of FeCrAl alloys [3,8–11]. The body-centered-cubic (BCC) structure of FeCrAl alloys remains stable from the melting point to room temperature, as the high content of Cr and Al. The single structure of FeCrAl alloy without allotropic transformation indicates that it is difficult to refine grains through phase transformation as in carbon steels [12,13]. The LWRs fuel cladding requires a thin-walled seamless tube with a diameter of ~10 mm, wall thickness ≤ 0.5 mm, and a length of ~4 m [14]. The main manufacturing process of commercial fuel cladding tubes includes drawing and pilgering techniques [14]. Yamamoto et al. [15,16] successfully prepared seamless Fe-13Cr-5.2Al-0.05Y-2Mo steel tubes using the drawing method. However, the cladding tube has coarse grains and low dimensional accuracy. They also found that the accumulation of internal stress in the steel tube and the absence of intermediate annealing caused the tube to fracture after multiple drawings. These results indicate that heat treatment and processing are the most important factors affecting the final properties of the FeCrAl alloy cladding tube. Warm-pilgered rolling effectively reduces metal deformation resistance, creates sub-microstructure, increases the production rate and yield. Annealing treatment is required to restore their deformability and prohibit continuous reduction processes without premature failures.

* Corresponding author at: School of Materials Science and Engineering, Central South University, Changsha 410083, China.
** Corresponding author.
E-mail addresses: liuhuiqun@csu.edu.cn (H. Liu), zhang_ruiqian@126.com (R. Zhang).

https://doi.org/10.1016/j.jnucmat.2022.153575
0022-3115/

Deformed metals mainly undergo recovery, recrystallization, as well as grain growth stages during the recrystallization annealing process. Recovery involves thermally activated motion, agglomeration of point defects and moreover annihilation and rearrangement of dislocations [17,18]. After recovery, primary static recrystallization occurs, and the deformed structure is replaced by the newly formed dislocation-free equiaxed grains. As the annealing process progresses, the abnormal coarsening recrystallized grains begin to occur [18]. The recrystallization behavior of FeCrAl alloy has been researched in many Ref. [19–21]. Sun et al. [19] found that α, γ and <100>//ND fibers were mainly present in FeCrAl plates, the Nb-containing Laves phase could stabilize microstructures of recovery and recrystallization and weakened the recrystallized γ-fiber. Zhang et al. [20] concluded that as Nb content increased, so did the number density of the Fe_2Nb-type Laves phase and the recrystallization temperature, and the recrystallization grains were refined. Liang et al. [21] results show that the recrystallization rate increases with increasing annealing temperature and rolling reduction. These studies focus on the recrystallization behaviors of plates, while there are few reports on the recrystallization behavior of warm-pilgered FeCrAl alloy tubes. Therefore, in order to understand microstructural and textural evolutions of cladding tubes during annealing, research on the recrystallization behavior of the warm-pilgered FeCrAl alloy tube is necessary.

In this study, the recrystallization and texture evolutions in the two directions (axial and circumferential directions) of the warm-pilgered FeCrAl tube were investigated after annealing at 850 °C. The recrystallization kinetics and the evolution of mechanical properties were conducted by hardness testing. Electron Back-Scattered Diffraction (EBSD) was characterized the microstructural and textural evolutions. Scanning electron microscopy (SEM) was used to characterize the effect of Laves phase on the microstructure in the matrix. This work aims to understand the recrystallization behavior of warm-pilgered FeCrAl cladding tube and give some possible references for actual manufacture.

2. Materials and methods

The warm-pilgered FeCrAl tube was provided by Nuclear Power Institute of China. Table 1 listed the chemical composition of the FeCrAl alloys, which was analyzed using inductively coupled plasma atomic emission spectroscopy (ICP-AES). The FeCrAl tube is pilgered rolling at 650 °C with an outer diameter of 25 mm and a thickness of 1.8 mm. The specimen was taken from the middle of the tube using electric discharge machining. Axial direction (AD), tangential direction (TD) and radial direction (RD) were defined as rolling, tangential and normal directions of the tube, respectively.

Different specimens cut from the warm-pilgered FeCrAl tube were annealed 1 h for different temperatures to determine the recrystallization temperature. The warm-pilgered FeCrAl tube was annealed for different times to investigate the recrystallization kinetics, microstructural and textural evolution. The muffle furnace was calibrated before heat treatment. Vickers hardness measurements were conducted using an HVS-1000 Micro Hardness Tester with a load of 1 kg and a dwell time of 10 s. The hardness values HV1±ΔHV1 were obtain from the averages over seven indents with a standard deviation ΔHV1. When testing EBSD data, the sample is positioned to analyze the evolution of texture during recrystallization.

Table 1
Chemical composition of FeCrAl alloys (wt%).

Element	Cr	Al	Mo	Nb	Ti	Zr	Si	Fe
Content	12.5	3.75	1.8	0.98	0.19	0.02	0.23	Balance

Backscattered electron imaging was used to characterize the Laves phase and grains in a TESCAN MIRA3 FE-SEM. The accelerating voltage was set at 20 kV, and the working distance was ~ 15.1 mm. EBSD data was collected using a JEOL 7900F FE-SEM coupled with an Oxford C-nano collection system. The extracted data including the average grain size, grain boundaries, aspect ratio and texture was analyzed using the HKL* Channel 5 data analysis software package. Grain boundaries with misorientation angle lower and higher than 15° were defined as low-angle grain boundaries (LAGBs) and high-angle grain boundaries (HAGBs), respectively. The texture component analysis was estimated with an orientation tolerance of 15° The orientation distribution function (ODF) in Euler space was used to visualized describe crystallographic texture. Texture results were generated using the series expansion method [22] with an Lmax of 22 and a Gaussian half width of 5°

3. Results and discussion

3.1. Microstructure of warm-pilgered FeCrAl tubes

Fig. 1(a) shows a 3D-orientation image map of the warm-pilgered sample colored according to a reference inverse pole figure shown as the standard triangle. As indicated, the warm-pilgered FeCrAl tube clearly shows obvious anisotropy in grain orientation and morphology. In the cross-section (TD-RD) plane of the tube, almost all the grains with a <110> direction (in green) along the axial direction, indicating that the warm-pilgered tube has a strong α-fiber (<110>//AD). However, there are many elongated grains colored blue parallel to the radial direction (<111>//RD) in the longitudinal planes of the tube. In fact, α-fiber and γ-fiber often appear in the process of cold rolling FeCrAl alloy [19–21,23]. Furthermore, most of the grains show orientation color transition and deformation bands, indicating a lot of deformation and substructures of the internal grains. To investigate the deformation structure, the grain boundary (GB) map is displayed in Fig. 1(b). The GB map reveals that there are many grains with high local misorientation angles inside can be found. Furthermore, an abundance of LAGBs predominance over HAGBs can be observed in the deformation structures. Many of dislocations and substructures within the deformed grains during warm-rolling can be well rationalized. In the warm-pilgered process, most of the energy is dissipated as heat energy, which accelerates the diffusion of point or line defects (mainly dislocations) in the deformed grains. Dislocation annihilation and rearrangement lead to the formation of these subgrains. On the other hand, under the action of shear stress, the movement of dislocations along the slip surface will encounter various obstacles, such as grain boundaries, precipitated particles, which hinder the movement of dislocations and cause dislocation entanglement. The low dislocation density regions are separated by

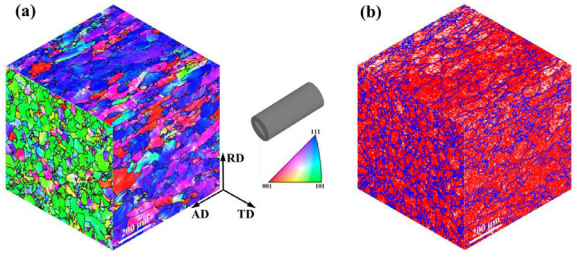

Fig. 1. 3D-EBSD microstructure of the warm-pilgered tube, (a) inverse pole figure (IPF) map, (b) grain boundary map (blue and red lines correspond to HAGBs and LAGBs, respectively). (For interpretation of the references to colour in this figure legend, the reader is referred to the web version of this article.)

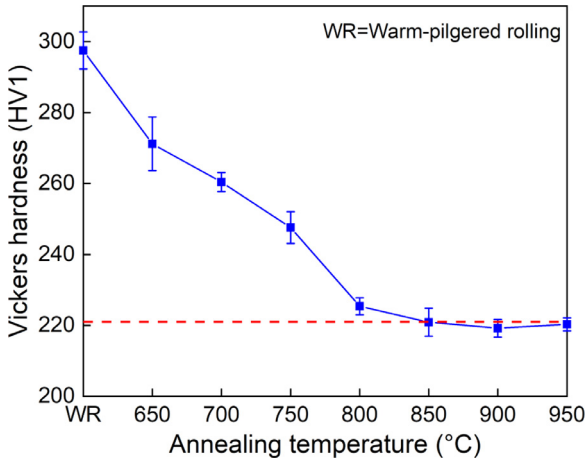

Fig. 2. Vickers hardness vs annealing temperature in the warm-pilgered tube after 1 h anneals at temperatures between 650 °C and 950 °C. Based on hardness varies with temperature, the recrystallization temperature is inferred to be 850 °C.

a high density of entangled dislocations, and these regions are deformed subgrains [20].

3.2. Recrystallization temperature of the warm-pilgered FeCrAl tube

To determine the recrystallization temperature of the warm-pilgered FeCrAl tube, isochronal 1 h anneals of the warm-pilgered tube were carried out at temperatures ranging from 650 °C to 950 °C. The resulting Vickers hardness is shown in Fig. 2, where the Vickers hardness stabilizes at 850 °C. Therefore, we conclude that the recrystallization temperature of the warm-pilgered FeCrAl tube is 850 °C.

3.3. Recrystallization kinetics of the warm-pilgered FeCrAl tube

In Section 3.1, we know that the warm-pilgered tube has obvious anisotropy in the tube axial and circumferential direction, so it is necessary for us to analyze the recrystallization behavior in these two directions. The changes in Vickers hardness of isothermal annealing at 850 °C for different time are shown in Fig. 3(a). The hardness of warm-pilgered tube has obvious anisotropy, and the hardness of cross-section is significantly less than that of longitudinal section. After complete recrystallization, the hardness did not decrease with the increase of annealing time, and a continuous platform appeared on the curve. A sharp drop in hardness indicates that recrystallization occurred, and the time for complete recrystallization was approximately 60 min. As the annealing time increased, the recrystallized grain growth stage did not occur, indicating that the grain of the alloy was stable at 850 °C. The initial hardness decreased sharply with annealing time, following a typical S-shaped evolution. To quantitatively assess the recrystallization kinetics, the relationship between hardness and annealing time was defined as the recrystallized volume fraction X analogous to [24] as follows:

$$X = \frac{HV_{WR} - HV_t}{HV_{WR} - HV_{rex}} \quad (1)$$

where HV_{WR} is the hardness of the warm-pilgered state, HV_t and HV_{rex} are the hardness at the annealing time t and the fully recrystallized state, respectively.

Fig. 2(b) shows the recrystallization volume fraction X as a function of the annealing time obtained from hardness testing using Eq. (1). The Johnson-Mehl-Avrami-Kolmogorov (JMAK) model [25] quantitatively describes the recrystallization kinetics using the relationship (Eq. (2)):

$$f = 1 - \exp(-kt)^n \quad (2)$$

Here k is the temperature-dependent kinetic coefficient, and Avrami exponent n [26] reflects the nucleation and growth of recrystallized grains.

In the JMAK equation, the values of k and n were obtained using nonlinear fitting in this study. Traditionally, continuous or site-saturated nucleation, and three-dimensional growth of recrystallization at a constant rate, the value of n is 3 to 4 [18]. The Avrami exponent n (axial and circumferential direction n_{AD} = 1.10 and n_{CD} = 1.37, respectively) is approximately equal to 1, which is smaller than the theoretical value. This is because of the dynamic recovery occurring in the warm-pilgered specimen, which resulted in many substructured nuclei/grains in the original microstructure [18]. Meanwhile, the presence of many Laves phasein the warm-pilgered specimen, hinders the nucleation and growth of recrystallization. The effects of Laves phaseon the microstructure are discussed in Section 3.5.

3.4. Microstructural evolution

According to the recrystallization volume fractions versus annealing time curve, four different stages of recrystallization (annealing times 0, 20, 60, and 600 min) were selected to investigate the microstructure and texture using EBSD.

The microstructural evolution of the warm-pilgered FeCrAl tube during isothermal annealing at 850 °C is shown in Fig. 4. Fig. 4(a) and (e) show the axial and circumferential microstructure of the warm-pilgered tube, respectively. The coarse grains with <111> orientation are shown along the tube axial direction, including many deformed and sub-microstructures, while there are relatively

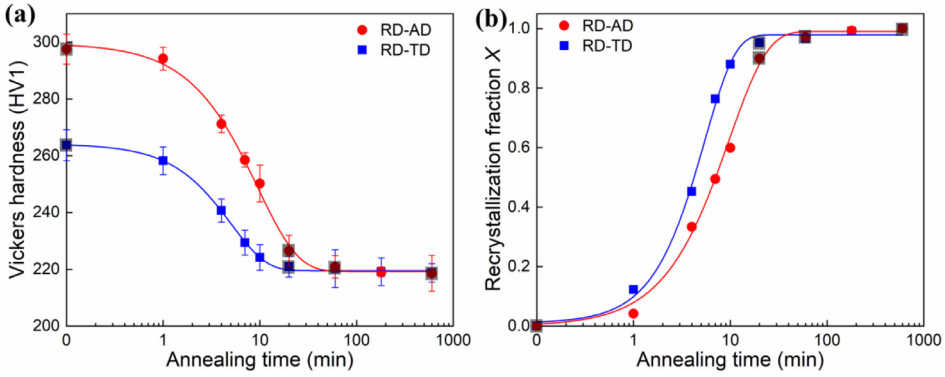

Fig. 3. Change of (a) Vickers hardness and (b) recrystallization fraction of warm-pilgered FeCrAl tube annealed at 850 °C for different times.

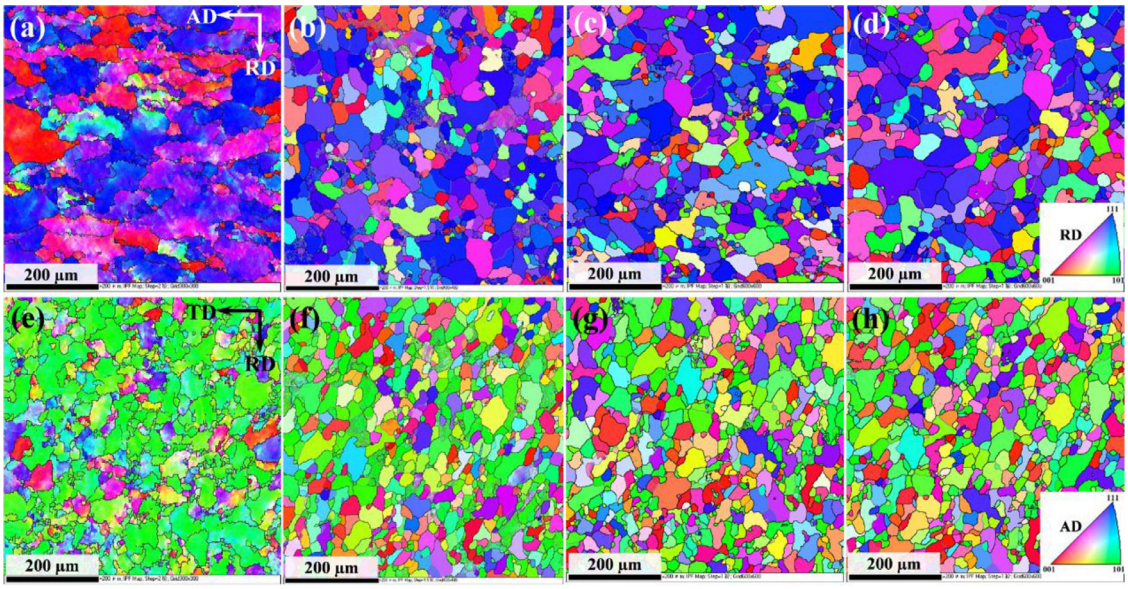

Fig. 4. IPF map of warm-pilgered FeCrAl tube annealed at 850 °C for different times: (a) (e) 0 min, (b) (f) 20 min, (c) (g) 60 min and (d) (h) 600 min. HAGBs (with misorientation angles higher 15°) shown as black lines and LAGBs (with misorientation angles between 2° and 15°) shown as gray lines. (For interpretation of the references to colour in this figure legend, the reader is referred to the web version of this article.)

Table 2
Statistical measures for average grain size and aspect ratio of all grains identified in different states of FeCrAl alloy tubes.

State	Detected grains number	Average grain size (μm)	Standard Deviation (μm)	Average aspect ratio (μm)	Standard Deviation (μm)
Warm-pilgered$_{(AD-RD)}$	275	30.8	42.2	2.1	0.90
Warm-pilgered$_{(TD-RD)}$	710	20.5	18.6	1.8	0.58
850 °C–20 min$_{(AD-RD)}$	577	24.2	19.0	1.8	0.70
850 °C–20 min$_{(TD-RD)}$	806	21.3	14.4	1.9	0.82
850 °C–60 min$_{(AD-RD)}$	779	20.3	17.0	1.8	0.71
850 °C–60 min$_{(TD-RD)}$	805	20.8	15.4	1.9	0.80
850 °C–600 min$_{(AD-RD)}$	586	24.3	18.8	1.8	0.70
850 °C–600 min$_{(TD-RD)}$	772	21.7	15.3	1.9	0.74
1200 °C–20 min$_{(AD-RD)}$	83	251.6	151.1	1.3	0.72

uniform grains with <110> orientation along the tube circumference. Fig. 4(b) and (f) illustrates the microstructure of the tube with an annealing time of 20 min, which contain a large number of recrystallized grains and few deformed structures, indicating that the recrystallization has been basically completed. This result is consistent with the recrystallization calculated by the hardness test in Fig. 3(b). When the annealing time was extended to 60 min, the microstructure in Fig. 4(c) and (g) contained most of recrystallized grains. After the tube was annealed at 850 °C for 600 min, as shown in Fig. 4(d) and (h) the microstructure is entirely composed of recrystallized grains without LAGBs. The absence of LAGBs in the grains indicates that complete recrystallization occurred. Therefore, holding for 60–600 min at 850 °C resulted in complete recrystallization.

Table 2 lists the average grain size and aspect ratio in different states of warm-pilgered FeCrAl tubes corresponding to Fig. 4 and Fig. 5. The average grain size and aspect ratio in axial direction of the warm-pilgered tube are approximately 30.8 μm and 2.1, respectively. The grains are significantly refined and the aspect ratio is reduced during recrystallization. After complete recrystallization, as the annealing time increases, the recrystallized grains and the aspect ratio remain stable at ~22 μm and 1.8, respectively. In order to verify the influence of Laves phase on the microstructure, we carried out heat at 1200 °C (above the re-dissolution temperature of Laves phase) for 20 min. The results indicate that the average

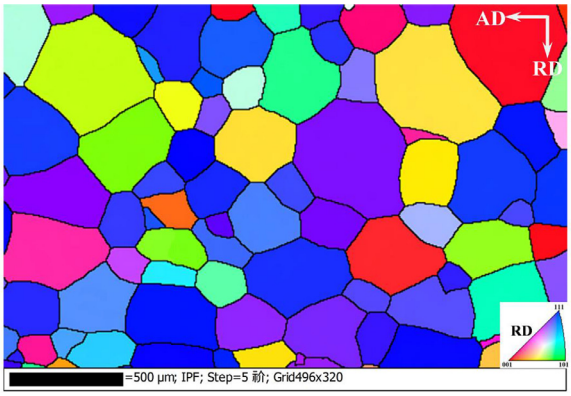

Fig. 5. IPF map of warm-pilgered FeCrAl tube annealed at 1200 °C for 20 min.

grain size is approximately 251.6 μm, which is much larger than that of the warm-pilgered state, and the aspect ratio in Fig. 5 is approximately 1.3 isometric shapes.

Fig. 6 shows the grain boundary misorientation angle distribution of warm-pilgered FeCrAl tube RD-TD plane annealed at 850 °C for different times. The warm-pilgered FeCrAl tube has a high proportion of LAGBs. The proportion of HAGBs increased and the contribution of the LAGBs decreased sharply during recrystallization.

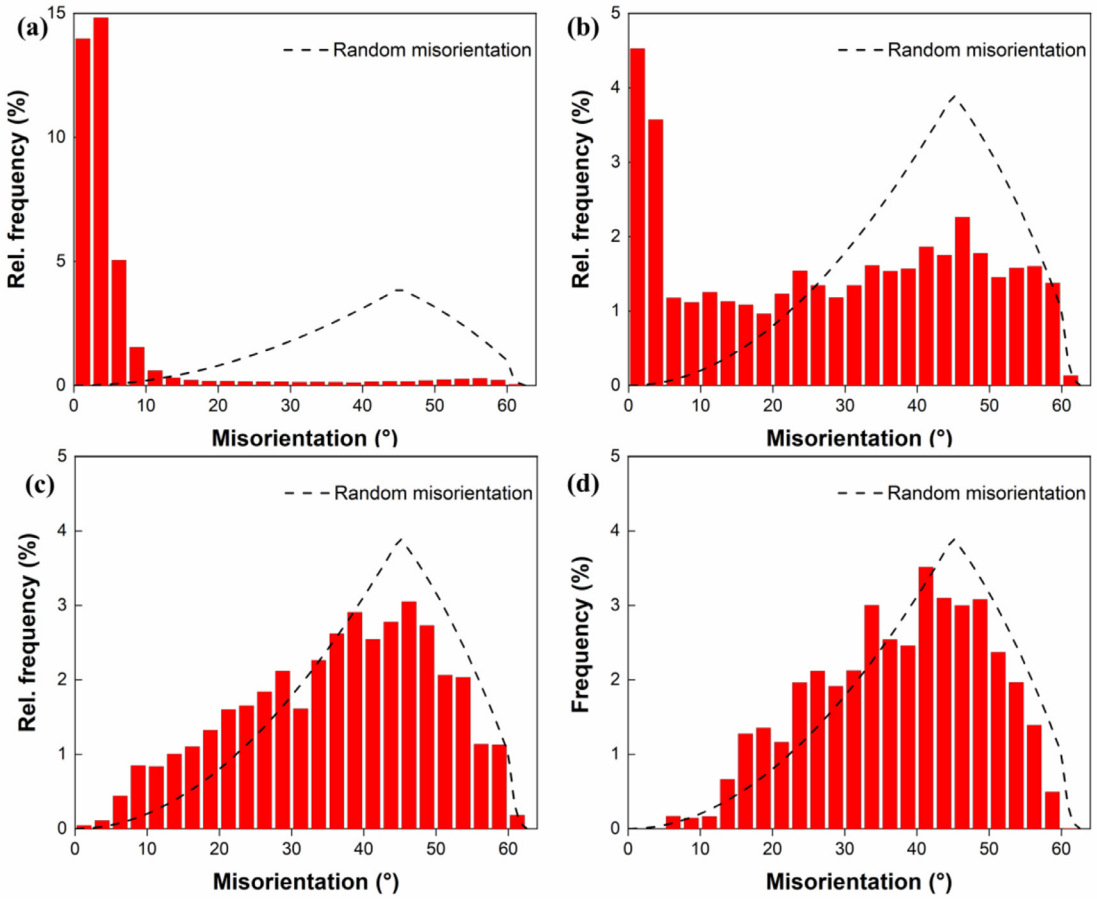

Fig. 6. The grain boundary misorientation angle distribution of warm-pilgered FeCrAl tube, (a) warm-pilgered sample and after annealing at 850 °C for different times: (b) 20 min, (c) 60 min, and (d) 600 min. The black dotted line represents a random misorientation (Mackenzie distribution) describing the misorientation angle distribution between completely random orientations considering cubic symmetry.

According to Ref. [27], the activation energy of HAGBs migration is approximately 3/5 of LAGBs. In the annealing process, LAGBs merged and migrated through the moving boundary [28] controlled by the atomic exchange to form HAGBs. After complete recrystallization, the grain boundary misorientation angle distribution approaches a Mackenzie distribution [29]. Certain deviations from the Mackenzie distribution in Fig. 6(d) caused by the texture of the tube can still be observed.

Fig. 7 quantifys the fraction of the LAGBs and CSL boundary of warm-pilgered tube during annealing. The LAGBs fraction of the warm-pilgered tube is 92.1%, which is consistent with the dominant low-angle grain boundarys in Figs. 1(b) and 6(a). The proportion of LAGBs decreases significantly with the increase of annealing time. When the annealing time is 600 min, the fraction of LAGB is 3.8%, which is close to the random orientation fraction 2.4%. The high fraction LAGBs is attributed to the formation of substructures during warm-pilgered rolling. Recrystallized grains nucleate and grow by consuming high-energy LAGBs. Therefore, the fraction of LAGBs decreases as deformed or recovered regions are replaced by recrystallized grains. The frequency of low-energy coincidence site lattice (CSL) can also be used to explain the evolution of the recrystallization during the annealing process. The warm-pilgered sample has a small amount of CSL (1.2%) frequency. As the annealing time increases, the frequency of CSL boundaries increases. This indicates that recrystallization is related to the formation of CSL. The CSL boundary is a low-energy grain boundary, which is thermodynamically stable. The grain boundary fraction of CSL is stable after recrystallization.

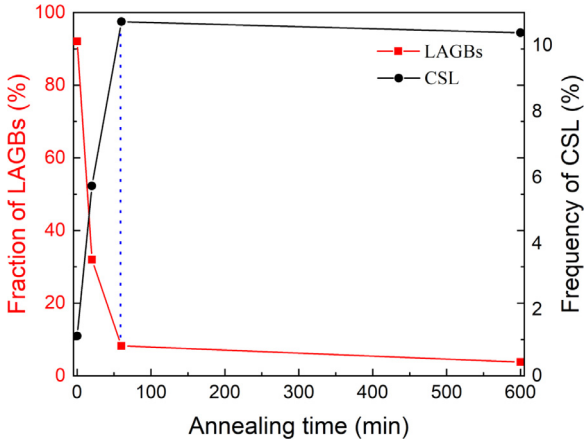

Fig. 7. Fraction of LAGBs and CSL of warm-pilgered FeCrAl tube after annealing for different times at 850 °C.

3.5. Laves phase

Fig. 8 exhibits BSE images of the warm-pilgered and annealed FeCrAl alloy tubes. The Laves phase(bright) are distributed along the rolling direction in warm-pilgered specimen. Occasionally, some cracks within the Laves phaseand debonding of the interface between matrix and the Laves phase are observed, as marked by black arrows in Fig. 8(a). After annealing at 850 °C for 20 min, the

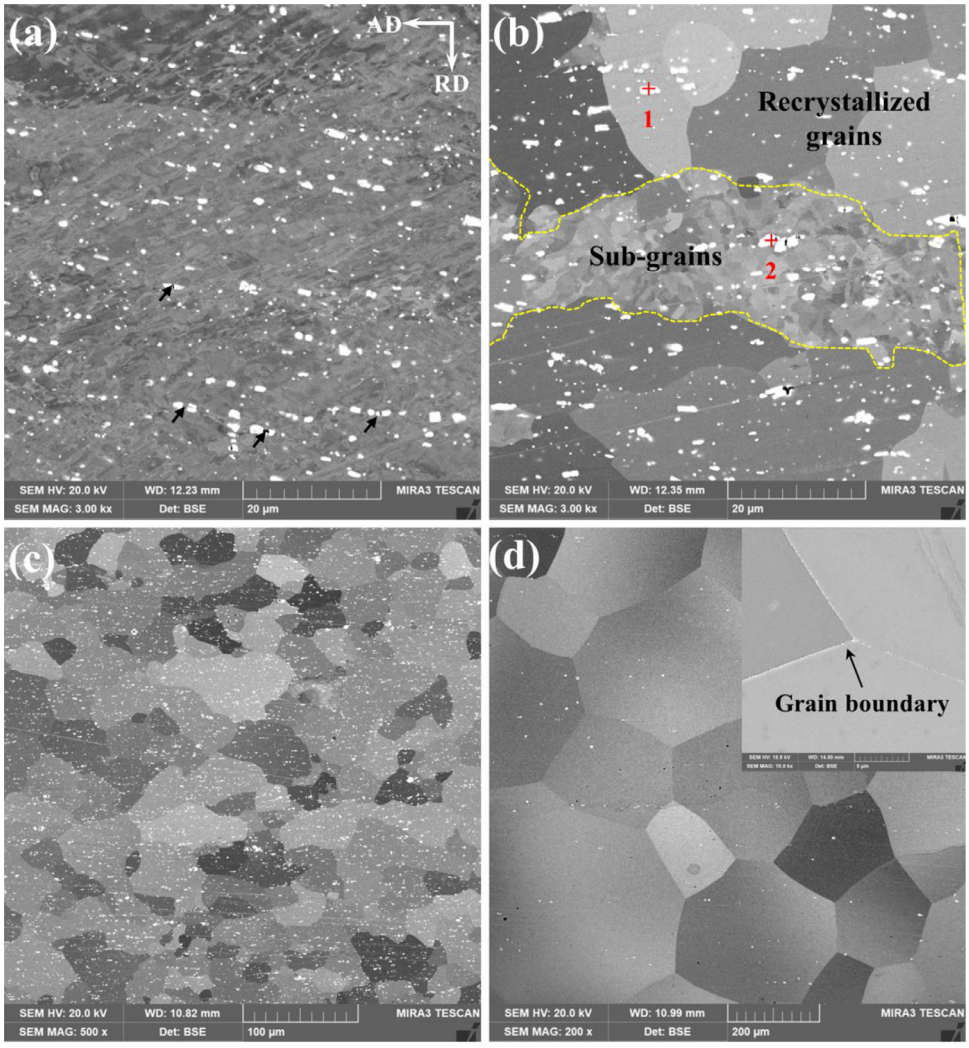

Fig. 8. BSE images of the warm-pilgered FeCrAl alloy tubes (a) and the specimen after annealing for (b) 20 min at 850 °C, (c) 600 min at 850 °C, and (d) 20 min at 1200 °C.

Table 3
Compositions of different locations in Fig. 8(b) determined by EDS (at%).

Location	Cr	Al	Mo	Nb	Ti	Si	Fe
1	10.49	3.39	4.34	13.57	0.87	2.95	64.39
2	12.94	5.28	2.96	14.72	0.78	2.15	61.18

warm-pilgered specimen recrystallized, and some sub-grains are surrounded by recrystallized grains. The large Laves phase (approximately 2 μm) is distributed in the matrix. In order to verify the composition of the Laves phase, the EDS analysis was performed as shown in Table 3. The Laves phase is mainly $(Fe, Cr)_2(Mo, Nb)$. No abnormal grain growth was observed despite holding at 850 for 600 min. When the annealing temperature was increased to 1200 °C, the Laves phase gradually re-dissolves into the matrix as shown in Fig. 8(d) inset. The average grain size was more than 200 μm. This indicates that these Laves phases can hinder grain boundary migration, resulting in stabiliziation of the microstructure and refinement of the recrystallized grains [19,20].

3.6. Textural evolution

To quantitatively describe textural evolution during annealing, the area fractions of α-fiber, and γ-fiber were calculated based on the texture components in the map. Fig. 9 shows the evolu-

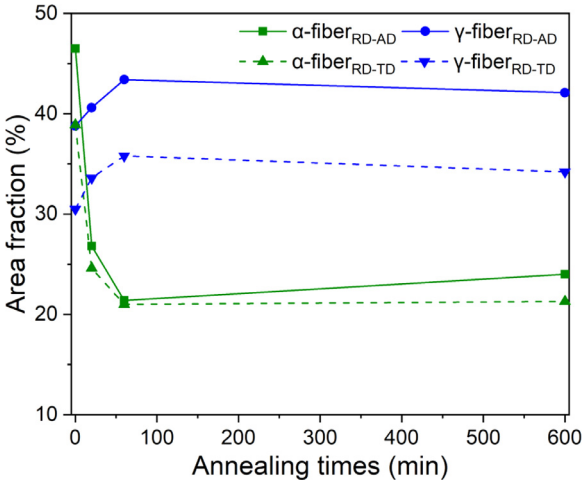

Fig. 9. The area fraction of main texture component/fiber changes with annealing time. The area fractions were calculated from the raw EBSD data obtained from the central region of the tube. The angular range of each component/fiber was defined as 15° from the ideal and the α-fiber was truncated in order to avoid any cross-over with the rotated cube component and γ-fiber.

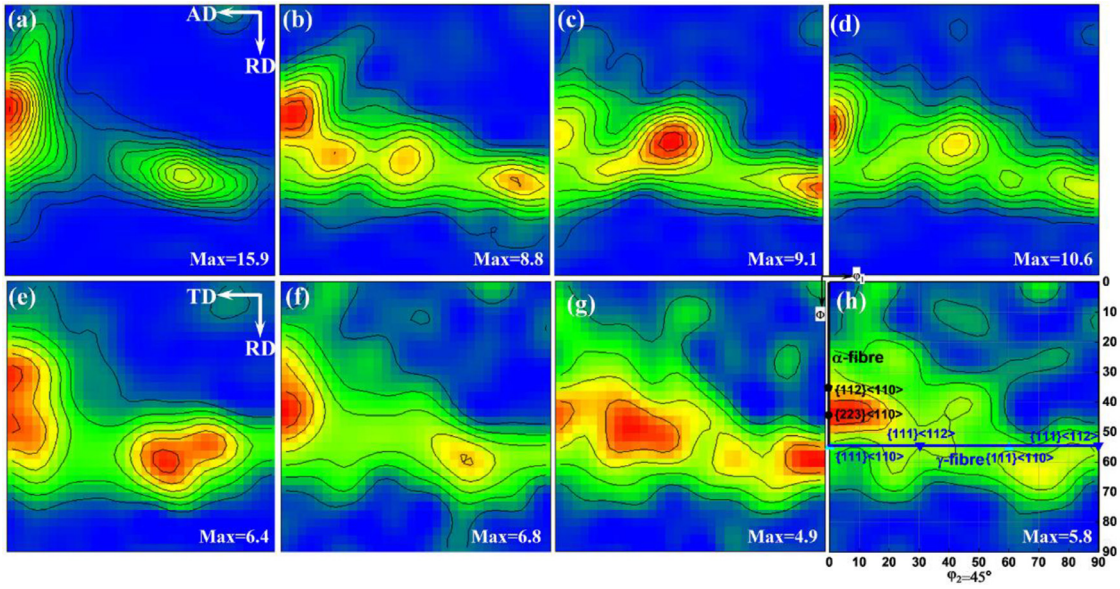

Fig. 10. $\varphi_2 = 45°$ ODF maps of (a) and (e) the warm-pilgered FeCrAl alloy tubes and specimens after annealing at 850 °C for (b) (f) 20 min, (c) (g) 60 min, and (d) (h) 600 min. Contour levels is 1,2,3,4.

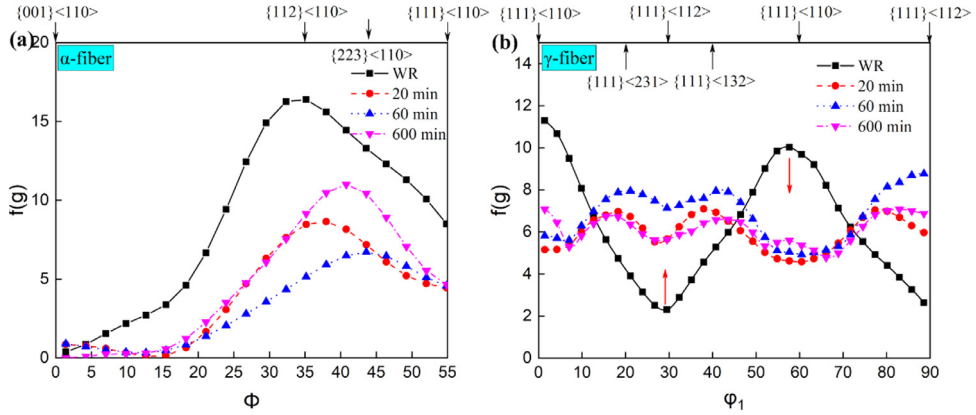

Fig. 11. F(g) from (a) α-fiber and (b) γ-fiber during the warm-pilgered FeCrAl alloy tubes after annealing at different times ($\varphi_2 = 45°$ section of ODF).

tion of the area fraction of α-fiber and γ-fiber as a function of the annealing time. It can be seen that the warm-pilgered tube has a strong α-fiber texture both in the AD-RD and TD-RD planes. The anisotropy results in a higher area fraction of α-fiber in AD-RD plane than in TD-RD plane. As the annealing time increases, the α-fiber area fraction decreases significantly while that of γ-fiber increases. This indicates that the initial α-fiber of the warm-pilgered tube has instability, which changes to the recrystallized γ-fiber during annealing. However, the texture fractions of the two fibers tends to be stable after recrystallization.

Fig. 10 illustrates the $\varphi_2 = 45°$section ODF maps for the warm-pilgered tube and specimen annealed at 850 °C for different annealing times. The warm-pilgered specimen exhibits typical rolled textures consisting of α-fiber and γ-fiber, which are consistent with body-centered cubic metals [24–27]. Fig. 10(a) and (e) shows the warm-pilgered condition of the $\varphi_2 = 45°$ ODF map, which is mainly composed of α-fiber and γ-fiber textures. In the AD-RD or TD-RD plane of the tube, α-fiber and γ-fiber are distributed throughout the orientation, but the texture intensity in the RD-AD plane is about twice that of RD-TD plane. As we all know, the slip system of bcc structural materials is {110}<111>. During the rolling process, the grains are more likely to rotate along the sliding plane {110} or the sliding direction <111>. In the pilger rolling process, the axial elongation of tube is achieved by the reduction of the cross section. The reduction of the cross section is achieved by the reduction of the tube diameter (R_D), the reduction of the wall thickness (R_W) or a combination of the two. The study found that the Q value (ie. R_W/R_D) plays a decisive role in reducing the diameter and wall deformation of the tube. The Q value is calculated as follows:

$$Q = \frac{R_W}{R_D} = \frac{(t_0 - t)/t_0}{(d_0 - d)/d_0} \tag{3}$$

where, t_0 and t are the tube wall thicknesses before and after rolling, respectively. d_0 and d are the tube average outer diameters before and after rolling, respectively. The dimensions of the tube before and after rolling in this experiment are as follows: $\Phi 33 \times 2.4$ mm $\rightarrow \Phi 25 \times 1.8$ mm. The Q value calculated according to formula (3) is 1.03, which is approximately equal to 1. As a result, the texture intensity in the AD-RD plane is higher than the texture intensity in the TD-RD plane. It is worth noting that the overall texture strength decreases during the recrystallization process. After annealing for 600 min, the α-fiber strong point texture component {112}<110> turns to {223}<110>. This suggests that the texture component {223}<110> has very high thermal stability.

Fig. 11 represents the change in the f(g) of the α-fiber and γ-fiber in the warm-pilgered tube and after annealing for different times at 850 °C. Obviously, the warm-pilgered tube has a strong γ-fiber strong point texture component {111}<110> and α-fiber strong point texture component {112}<110>, which has Euler angles $\varphi_1 = 0°$, $\Phi = 35°$, and $\varphi_2 = 45°$ The α-fiber orientation density gradually decreased with increasing annealing time. During the annealing process, γ-fiber texture component {111}<110> texture transform to new texture of {111}<112> texture by 30° rotation from crystalline direction of <110> to new direction of <112> which is consistent with FeCrAl ODS cladding tubes [30]. This second crystalline rotation resulted in formation of new γ-fiber with invariant {111} plane. A double-pole γ-fiber was found during annealing, with the main component {111}<231> and {111}<132>.

4. Conclusions

In this study, the 3D microstructure of warm-pilgered FeCrAl alloy tubes shows obvious anisotropy. Based on the obvious anisotropy of warm-pilgered tubes, we used EBSD and Vickers hardness tests to investigate the recrystallization behavior and texture evolution of the tube in the axial and circumferential directions. FeCrAl alloy tube first undergoes discontinuous recrystallization and then a slow recrystallization later stage. A modified JMAK equation was used to describe the recrystallization behavior during annealing. The anisotropy of the tube results in different recrystallization kinetic curves in the axial and circumferential directions. The distribution of fine Laves phasein the matrix inhibits the growth of recrystallized grains and delays recrystallization. The results of the quantitative texture analysis showed that the warm-pilgered FeCrAl alloy tube presented a strong α-fiber and γ-fiber. During the recrystallization process, the α-fiber texture intensity and area fraction are significantly reduced, the strong point texture component {112}<110> transforms into {223}<110>. The γ-fiber component {111}<110> transforms into {111}<112>. Recrystallization behavior and texture evolution of warm-pilgered FeCrAl tubes provide certain guidance for the heat treatment process of the cladding tube.

Declaration of Competing Interest

The authors declare that they have no known competing financial interests or personal relationships that could have appeared to influence the work reported in this paper.

CRediT authorship contribution statement

Xiao Qin: Investigation, Validation, Data curation, Conceptualization, Methodology, Writing – original draft, Writing – review & editing. **Zhe Liu:** Investigation. **Huiqun Liu:** Conceptualization, Writing – review & editing, Supervision, Funding acquisition. **Ruiqian Zhang:** Validation, Funding acquisition. **Qiangfu Pan:** Validation. **Yurong Wang:** Validation. **Jingyuan Pei:** Validation.

Acknowledgment

This research was funded by the Key Project of Nuclear Safety and Advanced Nuclear Technology (2019YFB1901002), “the Project supported by the State Key Laboratory of Powder Metallurgy”, Central South University, Changsha, China.

References

[1] J.A. Cairns, R.S. Nelson, G.K. Acres, The evolution of Fecralloy® steel-based catalysts, Int. J. Mater. Eng. Appl. 1 (1979) 162–166, doi:10.1016/0141-5530(79)90005-0.
[2] C. Tang, A. Jianu, M. Steinbrueck, M. Grosse, A. Weisenburger, H.J. Seifert, Influence of composition and heating schedules on compatibility of FeCrAl alloys with high-temperature steam, J. Nucl. Mater. 511 (2018) 496–507, doi:10.1016/j.jnucmat.2018.09.026.
[3] R.B. Rebak, Chapter 5 – FeCrAl–iron–chromium–aluminum monolithic alloys, in: Accident Tolerant materials for Light Water Reactor Fuels, Elsevier, 2020, pp. 83–141, doi:10.1016/B978-0-12-817503-3.00005-5.
[4] P. Dong, R. Zhang, W. Hui, L. Chao, Y. Liu, Formation and stability of oxide layer in FeCrAl fuel cladding material under high-temperature steam, J. Alloy. Compd. 684 (2016) 549–555, doi:10.1016/j.jallcom.2016.05.145.
[5] J. Dong, H.G. Kim, J.Y. Park, I.J. Yang, J.H. Park, H.K. Yang, A study of the oxidation of FeCrAl alloy in pressurized water and high-temperature steam environment, Corros. Sci. 94 (2015) 459–465, doi:10.1016/j.corsci.2015.02.027.
[6] M. Moalem, D.R. Olander, Oxidation of zircaloy by steam, J. Nucl. Mater. 182 (1991) 170–194, doi:10.1016/0022-3115(91)90428-A.
[7] S.S. Raiman, K.G. Field, R.B. Rebak, Y. Yamamoto, K.A. Terrani, Hydrothermal corrosion of 2nd generation FeCrAl alloys for accident tolerant fuel cladding, J. Nucl. Mater. 536 (2020) 152221, doi:10.1016/j.jnucmat.2020.152221.
[8] M.N. Gussev, K.G. Field, Y. Yamamoto, Design, properties, and weldability of advanced oxidation-resistant FeCrAl alloys, Mater. Des. 129 (2017) 227–238, doi:10.1016/j.matdes.2017.05.009.
[9] Y. Yamamoto, B.A. Pint, K.A. Terrani, K.G. Field, Y. Yang, L.L. Snead, Development and property evaluation of nuclear grade wrought FeCrAl fuel cladding for light water reactors, J. Nucl. Mater. 467 (2015) 703–716, doi:10.1016/j.jnucmat.2015.10.019.
[10] Z. Sun, H. Bei, Y. Yamamoto, Microstructural control of FeCrAl alloys using Mo and Nb additions, Mater. Charact. 132 (2017) 126–131, doi:10.1016/j.matchar.2017.08.008.
[11] Z. Sun, Y. Yamamoto, C. Xiang, Impact toughness of commercial and model FeCrAl alloys, Mater. Sci. Eng. A 734 (2018) 93–101, doi:10.1016/j.msea.2018.07.074.
[12] R. Rana, C. Liu, R.K. Ray, Low-density low-carbon Fe-Al ferritic steels, Scr. Mater. 68 (2013) 354–359, doi:10.1016/j.scriptamat.2012.10.004.
[13] O. Kubaschewski, Iron-Binary Phase Diagrams, Springer-Verlag Berlin Heidelberg, 1982 https://link.springer.com/book/10.1007/978-3-662-08024-5#toc.
[14] Y. Yamamoto, M.N. Gussev, B. Kim, T.S. Byun, Optimized Properties on Base Metal and Thin-Walled Tube of Generation II ATF FeCrAl, Oak Ridge National Laboratory, Oak Ridge, USA, 2015, doi:10.2172/1214036.
[15] D. Pociecha, B. Boryczko, J. Osika, M. Mroczkowski, Analysis of tube deformation process in a new pilger cold rolling process, Arch. Civ. Mech. Eng. 14 (2014) 376–382, doi:10.1016/j.acme.2014.01.001.
[16] Y. Yamamoto, Z. Sun, B.A. Pint, K.A. Terrani, Optimized Gen-II FeCrAl Cladding Production in Large Quantity for Campaign Testing, Oak Ridge National Laboratory, Oak Ridge, USA, 2016, doi:10.2172/1257911.
[17] R.D. Doherty, D.A. Hughes, F.J. Humphreys, J.J. Jonas, D. Juul Jensen, M.E. Kassner, W.E. King, T.R. McNelley, H.J. McQueen, A.D. Rollett, Current issues in recrystallization: a review, Mater. Sci. Eng. A 238 (1997) 219–274, doi:10.1016/S0921-5093(97)00424-3.
[18] J. Humphreys, G.S. Rohrer, A. Rollett, Recrystallization and Related Annealing Phenomena, 3rd ed., Elsevier, 2017.
[19] Z. Sun, P.D. Edmondson, Y. Yamamoto, Effects of Laves phase particles on recovery and recrystallization behaviors of Nb-containing FeCrAl alloys, Acta Mater. 144 (2017) 716–727, doi:10.1016/j.actamat.2017.11.027.
[20] Y. Zhang, H. Wang, H. Sun, G. Chen, Effects of annealing temperature on the microstructure, textures and tensile properties of cold-rolled Fe–13Cr–4Al alloys with different Nb contents, Mater. Sci. Eng. A 798 (2020) 140236, doi:10.1016/j.msea.2020.140236.
[21] X.L. Liang, H. Wang, Q.F. Pan, J.Y. Zheng, H.Q. Liu, R.Q. Zhang, Y. Xu, Y. Xu, D.Q. Yi, Recrystallization and mechanical properties of cold-rolled FeCrAl alloy during annealing, J. Iron Steel Res. Int. 27 (2020) 549–565, doi:10.1007/s42243-020-00387-z.
[22] M. Dahms, H.J. Bunge, The iterative series-expansion method for quantitative texture analysis. I. General outline, J. Appl. Cryst. 22 (1989) 439–447, doi:10.1107/S0021889889005261.
[23] Z. Sun, Y. Yamamoto, Processability evaluation of a Mo-containing FeCrAl alloy for seamless thin-wall tube fabrication, Mater. Sci. Eng. A 700 (2017) 554–561, doi:10.1016/j.msea.2017.06.036.
[24] A.A. Gazder, M. Sánchez-Araiza, J.J. Jonas, E.V. Pereloma, Evolution of recrystallization texture in a 0.78wt.% Cr extra-low-carbon steel after warm and cold rolling, Acta Mater. 59 (2011) 4847–4865, doi:10.1016/j.actamat.2011.04.027.
[25] M. Fanfoni, M. Tomellini, The Johnson-Mehl- Avrami-Kohnogorov model: a brief review, Nuovo Cimento D 20 (1998) 1171–1182, doi:10.1007/BF03185527.
[26] M. Avrami, Kinetics of phase change. I general theory, J. Chem. Phys. 7 (1939) 1103–1112, doi:10.1063/1.1750380.
[27] P.R. Rios, F. Siciliano, H.R. Sandim, R.L. Plaut, A.F. Padilha, Nucleation and growth during recrystallization, Mater. Res. 8 (2005), doi:10.1590/S1516-14392005000300002.
[28] P.R. Rios, F. Sicillano, H.R.Z. Sandim, R.L. Plaut, A.F. Padilha, Mater. Res. 8 (2005) 225–238, doi:10.1590/S1516-14392005000300002.
[29] J.K. Mackenzie, Second paper on statistics associated with the random disorientation of cubes, Biometrika 45 (1958) 229–240, doi:10.1093/biomet/45.1-2.229.
[30] S.M.S. Aghamiri, T. Sowa, S. Ukai, N. Oono, K. Sakamoto, S. Yamashita, Microstructure and texture evolution and ring-tensile properties of recrystallized FeCrAl ODS cladding tubes, Mater. Sci. Eng. A 771 (2020) 138636, doi:10.1016/j.msea.2019.138636.